CrossMark

ORIGINAL ARTICLE

# Catalytic hydroprocessing of lignin β-O-4 ether bond model compound phenethyl phenyl ether over ruthenium catalysts

B. Gomez-Monedero[1] · J. Faria[1,2] · F. Bimbela[3,4] · M. P. Ruiz[1,5]

**Abstract** The catalytic hydroprocessing of phenethyl phenyl ether (PPE), a model compound of one of the most significant ether linkages within lignin structure, β-O-4, has been studied. Reactions were carried out using two ruthenium-based catalysts, supported on different materials: 3.8 wt.% Ru/C and 3.9 wt.% Ru/Al$_2$O$_3$. Aiming at studying the reaction mechanism, experiments were carried out at 150 °C and 25 bar in H$_2$ atmosphere, with varying feed to catalyst mass ratios and reaction time. Differences between the relative importance of the steps of the mechanism were observed when using those two catalysts. The most significant finding was the predominance of the cleavage of C$_\beta$-O bonds compared to the cleavage of the C$_{aryl}$-O when using Ru/Al$_2$O$_3$ as catalyst; whereas with Ru/C, the two routes were nearly equivalent. It has been observed that the kinetic model describes the general tendencies of consumption and formation of the different products, but some over/under estimation of concentrations occurs. Finally, the effect of temperature was also explored by carrying out reactions at 100 and 125 °C, observing that decreasing temperature from 150 to 125 or 100 °C favored the dimer hydrogenation route versus the hydrogenolysis of the ether bonds.

## 1 Introduction

Biomass is regarded as a key option in the future of energy markets. Being the only renewable organic carbon source in nature, it possesses an enormous potential for its valorization in the form of fuels, chemicals, and energy [1–3]. Among the numerous catalytic approaches proposed for the valorization of lignocellulosic biomass [2, 4–8], catalytic depolymerization of lignocellulosic biomass and its components has been studied in order to obtain target chemicals [6, 9].

In this sense, reducing sugars such as glucose, which can be further upgraded to platform chemicals, have been produced from liquid- and solid-catalyzed hydrolysis of cellulose [4, 10]. Liquid acid catalysis has also been studied for the whole lignocellulosic biomass fraction, using raw materials such as wood chips, as well as solid acid catalysts [10]. Single-step processes, such as the one proposed by Matson et al. [8], have also been studied. Nonetheless, due to the recalcitrance of lignocellulosic biomass, many strategies for its catalytic valorization and depolymerization depend upon a previous stage to make each of the components of lignocellulosic biomass accessible for further processing [2]. In this way, cellulose, hemicellulose, and lignin are separated, applying a suitable treatment to each one of the fractions. Cellulose and hemicellulose can be hydrolyzed into sugars, which can be

✉ M. P. Ruiz
mpruizramiro@gmail.com

1 Abengoa Research, Campus Palmas Altas, c/ Energía Solar 1, 41014 Seville, Spain

2 Present address: Faculty of Science and Technology, Catalytic Processes and Materials, University of Twente, Enschede, The Netherlands

3 Grupo de Procesos Termoquímicos (GPT), Aragón Institute for Engineering Research (I3A), Universidad Zaragoza, Mariano Esquillor s/n, 50018 Zaragoza, Spain

4 Present address: Grupo de Reactores Químicos y Biorreactores, Applied Chemistry Department, Universidad Pública de Navarra, 31006 Pamplona, Spain

5 Present address: Faculty of Science and Technology, Sustainable Process Technology, University of Twente, Enschede, The Netherlands

🌀 Springer

further converted into ethanol through fermentation, or into other chemicals by a series of catalytic processes [4, 11, 12].

Lignin is the most recalcitrant part of lignocellulosic biomass [10]. It accounts for 10 to 35 wt. % of biomass and has the highest energy content (up to 40%) among the different biomass fractions [10, 13]. Large quantities of lignin-containing streams are produced in cellulosic bioethanol plants and pulp and paper manufacturers. While lignin is an abundant by-product stream, presently, its only route of valorization is combustion for heat and power generation [14, 15]. Due the high-energy content of lignin, the power and steam demands of the second-generation bioethanol plants are readily exceeded by the massive quantities of lignin produced [16]. For this reason, it is critical to develop revalorization strategies for the conversion of lignin into added value products that can diversify the biorefinery outputs and improve the profitability of the plant. Different strategies are being investigated for lignin valorization through catalytic routes, such as oxidation, acid-base catalysis, or hydroprocessing [17–24]. Regarding lignin catalytic depolymerization, reductive lignin depolymerization (i. e., hydroprocessing) is one of the most widely studied processes amid the different proposed strategies [20–22]. Considering the structure of lignin, composed mainly of aromatic rings linked by C-C and C-O ether bonds, the importance of catalysts with specificity to break C-O bonds is critical, given its larger abundance and higher lability when compared to C-C bonds [22]. Among the different C-O ether bonds in lignin, β-O-4-type linkages are the most abundant, with up to 50% out of the total, followed by α-O-4 (12%) and 4-O-5 (8%) linkages [25–29].

The aim of this study was to deepen our understanding of the hydrogenolysis reaction of lignin-model compounds by investigating the effect of the catalyst support on the selectivity and activity of the reaction. For this reason, we decided to evaluate the effect of two distinct supports (active carbon and alumina) for the Ru-catalyzed C-O hydrogenolysis reaction. This reaction has been studied using phenethyl phenyl ether (PPE), a model compound of one of the most significant ether linkages within lignin structure, β-O-4 [25–30], as a probe molecule. Developing fundamental structure/property relationships will be critical in the optimization of the catalyst design. On one hand, activated carbon is a porous material with high surface area that contains a significant number of oxygenated functional groups (e.g., -OH, -COOH, -COC, and CHO) with distinct acidity that are formed after activation treatments (e.g., steaming, acid washing, and oxidation). These functionalities can effectively coordinate metal complexes during catalyst synthesis, which leads to the stabilization of small metal clusters upon thermal treatment under reducing conditions [31–34]. On the other hand, gamma alumina has a smaller surface area, and the interaction with noble metal clusters is primarily due to charge transfer at the metal-support interface, in which free electrons of elemental Al are attracted to the metal [35, 36].

The results showed that on activated carbon, the catalyst activity was significantly higher in comparison to alumina. In terms of selectivity, the two catalyst were very selective towards the hydrogenolysis of the CO bond compared to hydrogenation of the aromatic ring. Nonetheless, the hydrogenolysis of $C_{aryl}$-O was significantly more favorable on Ru supported on active carbon than alumina. The differences in activity and selectivity were attributed to the smaller Ru cluster size on active carbon (4 nm) in comparison with gamma alumina (50 nm).

## 2 Experimental

**Materials and methods** Methanol, used as reaction solvent, was purchased from VWR (Methanol GPR RECTAPUR, ≥99.5%). Ru precursor was obtained from Sigma Aldrich ($RuCl_3$, 45–55% Ru content), together with the active carbon used as support (Activated Charcoal DARCO®, ~100 mesh particle size, Sigma-Aldrich). On the other hand, the aluminum oxide support was provided by Sasol ($Al_2O_3$, Martinswer (Albemarle), COMPALOX AN/V-813). The selected β-O-4 model compound, PPE, was prepared following the method proposed by Rensel et al. [37], in which 4 g of phenol (99% purity, ACROS Organics) was added to a bottom rounded flask together with 6 g of $K_2CO_3$ (99% minimum purity, ACROS Organics) and 33 mL of anhydrous acetone (synthesis grade, Fisher Chemical). After 1 h of reflux, 11 g of anhydrous (2-bromethyl)-benzene (Sigma Aldrich) was added to the mixture. After 24 h of reaction, 25 mL of ethyl ether and 25 mL of water were added. Ethyl acetate (99.8% purity, Sigma Aldrich) was used to extract the organic compounds, which were washed three times with a solution 1 M of sodium hydroxide (NaOH, reagent grade, 98% minimum purity, Sigma Aldrich) and another 1 M of sodium chloride (NaCl, 99.5%, ACROS Organics). Then, the ethyl acetate phase was evaporated in a rotary evaporator until only styrene, phenol, and phenethyl phenyl ether were left. The desired compound (PPE) was separated by flash chromatography using a mixture of hexane and ethyl acetate as eluent.

## 3 Experimental installation and procedures

Liquid-phase batch catalytic tests for hydroprocessing of PPE were carried out in a high-pressure stainless steel autoclave reactor (Berghof Highpreactor™ High-Pressure Laboratory Reactor BR100), equipped with a 50-mL teflon liner, a pressure transducer or two manometers (one for pressures up to 10 bar, the other for pressures up to 250 bar), a stainless-steel deposit for liquids, a thermocouple connected to a temperature controller, and a magnetic stirrer. To carry out the catalytic runs, a stock solution of PPE in methanol (16 mM) was prepared.

Prior to reaction, 40 to 70 mg of the desired catalyst was heated up to 250 °C for 1 h and under 15 mL/min of $H_2$ in a tubular quartz reactor. Once the target temperature was reached, the catalyst was reduced in situ at these conditions for 3 h. Then, the catalyst was passivated in an air flow (15 mL/min) at room temperature for 30 min. After this, 25 or 50 mg of the selected catalyst together with a magnetic stirrer was placed inside the 50 mL Teflon liner, the stainless-steel batch reactor was sealed, and a leak test was carried out at 50 bar-g in $N_2$ atmosphere. Then, the reactor was flushed three times with pure $H_2$ to remove any remaining $N_2$ from the leak test, and after this, the reactor was pressurized up to 7–8 bar-g using $H_2$. The reaction system was heated up to the desired temperature (100, 125, or 150 °C) with a heating rate of approximately 1.5 °C/min and, once the target temperature was achieved, the system was maintained at this temperature and pressure for 30 min to activate the catalyst. Afterwards, 20 mL of stock solution of PPE was placed into the liquid's vessel of the reactor, which was subsequently pressurized to 25 bar-g using $H_2$. The discharge valve of the vessel was opened, and the solution together with $H_2$ were introduced into the reactor. The latter procedure was repeated until the pressure inside the reactor vessel reached 25 bar-g, and after this, the relative centrifugal force (RCF, calculated per Eq. 1) was set to 4.55 times g (stirring speed of 750 rpm). At this moment, reaction time was set to zero. After the desired time of reaction, the heating and stirring were stopped and the reactor was cooled down in an ice-cooled bath. When the reactor temperature was below 20 °C, it was carefully depressurized.

$$RCF = 1.1118 \times 10^{-5} \times r \times N_{rpm}^2 \qquad (1)$$

where $r$ is the rotational radius in centimeters and $N_{rpm}$ is the rotational speed measured in revolutions per minute (rpm).

Liquid products were filtered and analyzed using gas chromatography. The products obtained after reaction were analyzed by GC-MS for identification (Agilent 7890 GC-system, model G3440A, equipped with a 5975C mass spectrometer detector. Column: Agilent HP5-ms, 0.250 mm inner diameter, 30 m long, 0.25 μm film thickness) and by GC-FID for quantification (Agilent 7890 GC-system, model G3440A, equipped with a 5975C flame ionization detector. Column: Agilent HP5, 0.320 mm inner diameter, 30 m long, 0.25 μm film thickness).

After identification of the products, the sample was injected in the GC-FID system to quantify the obtained products with the aid of calibration curves previously prepared. Each curve contained eight concentration levels, from 1.2 mM to 50 mM, and response factors for each compound were obtained by adjusting the areas obtained at each concentration level, assuming that for concentrations equal to 0 mM, the corresponding response areas were 0 as well. Concentration levels were

prepared by producing first a stock solution with a concentration of 50 mM for each of the calibrated compounds in methanol, and diluting selected volumes of this solution to obtain the rest of concentrations. Each solution was injected three times, and the mean value of the obtained areas was calculated and used for fitting the curve.

Once the concentration of each product before and after reaction was calculated according to calibration curves, the yield to each product was determined. As several reactions were taking place at the same time (hydrogenation of the dimer, hydrogenolysis, etc.) conversion, selectivity and yields were calculated on a molar C basis. The defined equation for each parameter can be seen below (Eqs. 2–4).

$$\%Conversion = \frac{\text{mol C } of\ Dimer_0 - \text{mol C } of\ Dimer_f}{\text{mol C } of\ Dimer_0} \cdot 100 \qquad (2)$$

$$S_A = \frac{\text{mol C } of\ product\ A}{Total\ \text{mol C } of\ products} \qquad (3)$$

$$Y_A(\%) = S_A \cdot Conversion(\%) \qquad (4)$$

Being

- mol C of $Dimer_0$: the moles of carbons in the form of PPE in the solution before reaction.
- mol C of $Dimer_f$: the moles of carbon in the form of PPE in the solution after reaction.
- $S_A$: selectivity to product A, *i. e.* toluene.
- Total mol C of products: the sum of the moles of carbon of all the products detected by GC-FID.
- $Y_A$: yield to product A.

In addition, to ease comparison, some results were presented in the form of yield to four families of compounds: aromatic monomers (AM), saturated monomers (SM), partially saturated dimers (PSD), and fully saturated dimers (FSD). The group of AM included these molecules: benzene, toluene, phenol, and benzylethanol. The saturated monomers included the following compounds: cyclohexanone, cyclohexanol, ethylcyclohexane, cyclohexane, 2-cyclohexylethan-1-ol, methoxycyclohexane, and 1.1-dimethoxycyclohexane. Finally, 2-(cyclohexylethoxy)benzene and (2-(cyclohexyloxy)ethyl)benzene were the PSD, and (2-cyclohexylethoxy)cyclohexane was the FSD. Equation 5 exemplifies the calculation of the yield to one of the families.

$$Y_{aromatic\ monomers} = Y_{toluene} + Y_{phenol} + Y_{benzene} \cdots \qquad (5)$$

**Catalyst preparation** Ru catalysts (supported on active carbon and $Al_2O_3$) were synthesized by excess impregnation. The necessary amounts of Ru precursor salt ($RuCl_3$, 45–55% Ru

content, Sigma-Aldrich) were weighed and dissolved in the corresponding volume of deionized water to produce a catalyst with a content of the active metal equal to 5 wt. % in the final solid, following the proportion of 500 mL of water for 0.54 g of $RuCl_3$. The solution of the precursor in water was stirred at room temperature using a magnetic stirrer, until complete dissolution of the salt. Once the solution of $RuCl_3$ was homogeneous, the desired amount of support was added to the solution and the mixture was maintained under stirring overnight. Afterwards, the solution was heated to evaporate the water, and the solid obtained was dried in an oven at 100 °C overnight.

After impregnation and drying in an oven overnight, the catalysts were calcined as follows. $Ru/Al_2O_3$ catalyst was calcined in a muffle furnace in air atmosphere, with a temperature ramp of 3 °C/min up to 400 °C, and maintained at 400 °C for 4 h. Ru/C catalyst was calcined in a tubular quartz reactor, with a vertical flow of nitrogen of 20 N mL/min. A temperature ramp of 3 °C/min was set to reach 400 °C, and then, the solid was maintained at this temperature for 4 h under nitrogen flux.

**Catalysts characterization** Textural properties of these two catalysts were analyzed by the following techniques: temperature-programmed reduction (TPR), high-resolution transmission electron microscopy (HRTEM), and nitrogen adsorption isotherms (BET).

TPR analyses were carried out in a Micromeritics Chemisorption Analyzer (AutoChem II), equipped with TCD detectors. Samples were heated at 10 °C/min from room temperature to 800 or 900 °C, while a stream of 50 mL/min of 10% $H_2$-Ar mixture circulated through the system. High-resolution TEM images were acquired in a Tecnai F30 (FEI company) high resolution Transmission Electron Microscope that can work in either TEM or STEM (Scanning-Transmission) modes. Isotherms were determined in an ASAP 2020 system (Micromeritics). Prior to the analyses, samples were degasified under vacuum, applying a temperature program (10 °C/min ramp from room temperature to 200 °C, holding the latter temperature during 360 min). $N_2$-adsorption was carried out at 77 K by dosing growing amounts of $N_2$ to cover the whole relative pressures interval, until reaching a point close to saturation ($P/P_0 = 0.995$). Then vacuum was applied to progressively reduce pressure, producing desorption of the gas. Surface area was estimated using the Brunauer-Emmett-Teller (BET) model, applied to the adsorption branch at the selected partial pressures range for each catalyst, thus capillary condensation in mesopores was avoided.

# 4 Results and discussion

**Catalyst characterization** The results of nitrogen adsorption (BET) showed a value of surface area of 814.4 $m^2$/g for Ru/C catalyst, and 231.1 $m^2$/g for $Ru/Al_2O_3$. From HRTEM images

(Fig. 1(a.1), (a.2), (b.1), (b.2)), it was possible to determine the Ru particle size distribution and calculate average particle size of the unreduced catalysts. The particle size distribution curves were obtained from the detailed analysis of hundreds of particles from tents of images from distinct regions of the TEM-grid (Fig. 2). For Ru/C catalyst, the Ru average particle size was 4 nm, while in the $Ru/Al_2O_3$ catalyst, the value was much higher, ~50 nm. It seems clear that the higher surface area of the active carbon support favored the dispersion of the Ru particles, as it can be also observed from HRTEM images (Fig. 1(a.1), (a.2), (b.1), (b.2)). When using alumina as support, Ru particles tended to agglomerate on specific regions. We have measured the real amount of Ru deposited on the catalysts by X-Ray Microfluorescence. The results show a Ru content of 3.81 wt. % for Ru/C catalyst, and 3.93 wt. % for $Ru/Al_2O_3$.

It is important to mention that HRTEM images have been taken from the unreduced samples. Thus, some changes in the particle size or morphology may be expected after reduction or activation steps. While it is possible that absolute values of the cluster size could be different under reaction conditions, the relative differences observed in the HRTEM should resemble those of the working catalyst.

The TPR profiles of both catalysts are shown in Fig. 1(c). A remarkable difference in both profiles can be observed. While $Ru/Al_2O_3$ presented a main reduction peak at ~210 °C with a second peak at ~530 °C, Ru/C presented a double peak with maximums at ~170 and 240 °C with a broad peak at ~510 °C. The peak at 210 °C for $Ru/Al_2O_3$ may be attributed to the reduction of Ru oxides [38], and the peak at 530 °C to the reduction of Ru atoms having stronger interaction with the $Al_2O_3$ support [39]. In the Ru/C TPR profile, the double peak could be attributed to the $RuO_x$ species and bulk $RuCl_3$ [40], while the broad peak at 510 °C may be attributed to the partial gasification of the carbonaceous support [41, 42]. For comparison, the TPR profiles of both supports ($Al_2O_3$ and activated carbon) have been also included in Fig. 1. While on $Al_2O_3$, no reduction peaks were observed in the activated carbon, but a broad peak was observed centered at 530 °C associated to the gasification of carbon [41, 42]. Based on the TPR results, the split and the shift of the reduction peaks to lower temperatures on Ru/C may be attributed to the higher dispersion of Ru particles. In contrast, TPR on $Ru/Al_2O_3$ shows a single reduction peak at higher temperatures, which indicates that the larger particle size of the metal clusters makes the reduction less favorable. It may be possible that a $Ru/Al_2O_3$ catalyst with higher surface area, and thus higher dispersion, would have a lower temperature reduction peak.

It is worth noting that before the reaction, the catalyst is reduced in 60 bar of $H_2$ and 150 °C. The excess of hydrogen and that of temperature, in principal, would be enough to completely reduce the catalyst. However, it is possible that some Ru oxide particles are left, mainly if we take into

**Fig. 1** HRTEM images of Ru/C (*a.1* and *a.2*) and Ru/Al$_2$O$_3$ (*b.1* and *b.2*) unreduced catalysts, together with TPR profiles of both unreduced catalysts and the corresponding supports (*c*)
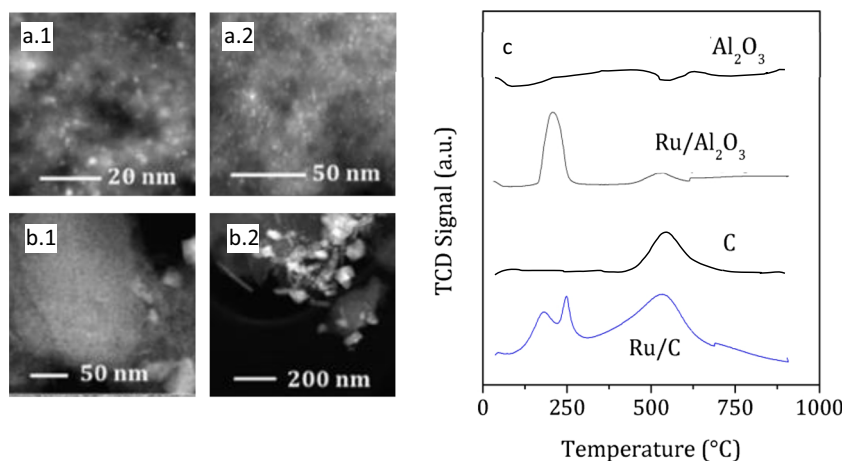


account the TPR results (Fig. 1c), where there is evidence that reduction temperatures for Ru/Al$_2$O$_3$ and Ru/C samples are at least 210 °C and 170–240 °C, respectively. Nevertheless, one could anticipate that this fraction is minimum, since the presence of Ru(0) nanoparticles would also co-catalyze the reduction of Ru oxide particles.

**Reaction network** To elucidate the reaction network for PPE, catalytic hydroprocessing runs were carried out in the presence of 3.8% Ru/C or 3.9% Ru/Al$_2$O$_3$ and using methanol as solvent. Several reactions were carried out at different values of mass of catalyst times total reaction time, $W \cdot t$, keeping the temperature as a constant at 150 °C. This parameter ($W \cdot t$) represents the amount of the selected catalyst for the reaction (in milligrams) times the reaction time (in hours). With this strategy, different conversion levels of the initial model compound were achieved. This, in addition, allowed observing the evolution of the different products or families of products with increasing conversion levels. Figure 2 presents the results obtained for 3.8% Ru/C and 3.9% Ru/Al$_2$O$_3$ in the hydroprocessing of PPE, grouped by families: AM, SM, PSD and FSD. AM includes phenol, benzene, ethylbenzene, and 2-phenylethan-1-ol. SM includes cyclohexanol, ethylcyclohexane, cyclohexane, and 2-cyclohexylethan-1-ol. PSD includes (2-cyclohexylethoxy)benzene and

(2-(cyclohexyloxy)ethyl)benzene. FSD includes (2-cyclohexylethoxy)cyclohexane.

Important differences in the relative importance of pathways between catalysts were observed. Notably, the hydrogenolysis pathway dominated over the competing hydrogenation reaction on both catalysts. As shown in Fig. 3, using both catalysts, the concentration of AM was higher than the concentration of partial hydrogenated dimers at low levels of conversion. This trend, however, diverted as the concentration increased; on Ru/C, the hydrogenolysis reaction dominated over the hydrogenation as the PPE conversion evolved, while in the case of Ru/Al$_2$O$_3$, the opposite trend was observed. These differences can be clearly observed when the ratio of C-O hydrogenolysis to hydrogenation reaction is calculated as a function of conversion (see Table 1). In the case of Ru/C, the ratio of hydrogenolysis/hydrogenation products starts at around 1.6 and progressively increased to 2.4 as the reaction evolved. On the contrary, on Ru/Al$_2$O$_3$, the ratio started at lower value, ca. 1.1, and progressively decreased to 0.4 when full conversion of PPE was achieved. To ease the comparison of both catalysts behavior, Fig. 4 shows the results of PPE and product concentration for the same reaction conditions (W·t = 100). It can be observed that at those conditions, Ru/C catalyst is much more active towards hydrogenation (higher SM and FSD concentrations) compared to Ru/
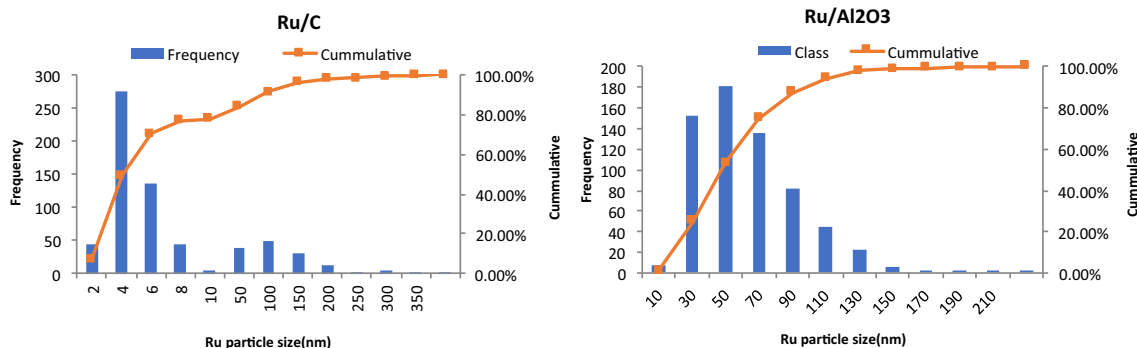


**Fig. 2** Distribution of Ru particle size in Ru/C (*left*) and Ru/Al$_2$O$_3$ unreduced catalysts (*right*), calculated from HRTEM images

**Fig. 3** PPE and product concentration (by family) variations with reaction time in the hydroprocessing of PPE (Reaction conditions: 25 bar-g of $H_2$, 150 °C). *Left*: reaction carried out with 3.8 wt. % Ru/C as catalyst. *Right*: reaction carried out with 3.9 wt. % Ru/$Al_2O_3$ as catalyst
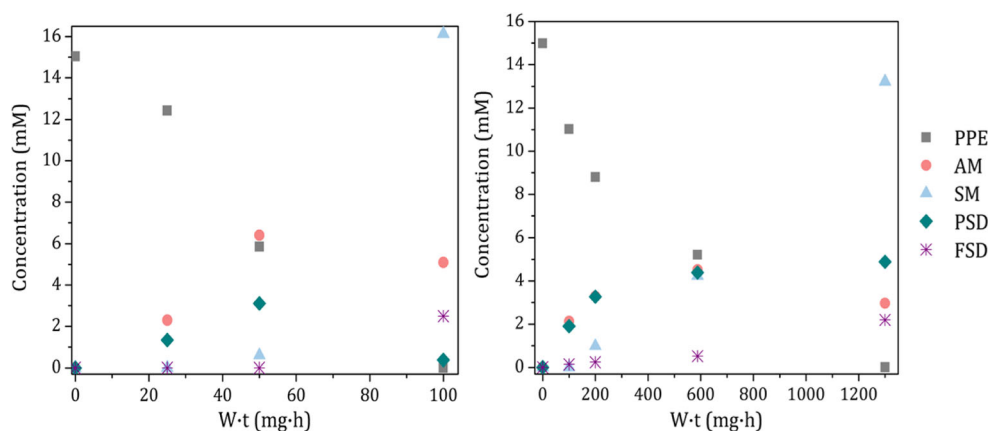


$Al_2O_3$. The higher concentration of SM and FSD on Ru/C is not caused by intrinsic differences in selectivity, but instead to the higher conversion level.

Based on these results, a reaction network was proposed (Fig. 5), in which the different products of the reaction were identified and quantified at each of the W·t levels studied for the two different catalysts. As can be seen in Fig. 5, the first step of the reaction was either the hydrogenation of one of the two aromatic rings of PPE ($k_3$ and $k_3'$) or the scission of the C-O bond. The latter can occur on the $C_{aryl}$-O bond ($k_1$) or the $C_\beta$-O bond ($k_2$). Then, aromatic monomers underwent hydrogenation ($k_4$ to $k_8$) yielding the corresponding saturated monomers. The route that produced methoxycyclohexane and 1.1-dimethoxycyclohexane, from cyclohexanone acetylation with methanol [43, 44], is also included in Fig. 5 ($k_9$ and $k_{10}$). Finally, partially saturated dimers were either hydrogenated to fully saturated dimers ($k_{11}$ and $k_{14}$) or their C-O bond was cleaved to yield the corresponding monomers ($k_{12}$, $k_{13}$, $k_{15}$, and $k_{16}$), which in the case of being aromatic compounds could be hydrogenated to their corresponding saturated forms.

Acidity of the catalysts may play an important role on the reaction pathways. This issue has been extensively studied for these catalysts by different authors [45–48], and it seems that there are not significant differences in acidity in the selected catalysts. However, in order to assure this fact and deeply analyze the effect of acidity in the reaction, some acidity measurements would be necessary.

In the case of PPE, it can be observed that C-O hydrogenolysis rate dominates over the competing hydrogenation reaction of the aromatic rings on both catalysts. As shown in Fig. 3, the concentration of PSD is always lower than the concentration of AM for any given conversion on Ru/C; while on Ru/$Al_2O_3$, the opposite trend is observed. This becomes more evident if the ratios of hydrogenolysis to hydrogenation reactions are compared for both catalysts (Table 1). The higher selectivity for C-O hydrogenolysis on the smaller particles could be attributed to the stronger interaction of the C-O bond to the low coordination sites of the smaller Ru clusters on the Ru/C catalyst. In contrast, in the larger Ru clusters, the flat-oriented adsorption of the aromatic ring is favored, which favors the saturation of the aromatic ring.

When the reaction was carried out with Ru/C as catalyst, PPE C-O bond was cleaved by pathways signaled by $k_1$ and $k_2$, with nearly the same importance of both. Conversely, in the case of the reactions catalyzed by Ru/$Al_2O_3$, the concentration of products obtained through the $k_2$ route was much more significant than the ones obtained through the $k_1$ route. The parameter $R$ was defined to illustrate this, as the ratio, at a given level of conversion, between the moles of products produced via $k_1$ pathway ($C_{aryl}$-O bond scission) and those produced via $k_2$, the latter corresponding to the pathway in which cleavage of the $C_\beta$-O bond occurs (Eq. 6). At low levels of conversion, each term of $R$ only contains the moles of

**Table 1** Ratio of hydrogenolysis to hydrogenation reactions on Ru/C and Ru/$Al_2O_3$ catalysts obtained for hydroprocessing of PPE in methanol. Reaction conditions: 25 bar-g of $H_2$, 150 °C

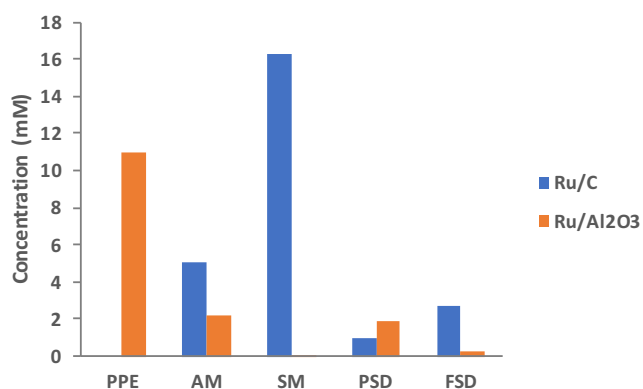| Catalyst | Hydrogenolysis products (mM) | Hydrogenation products (mM) | Ratio of hydrogenolysis/hydrogenation | Conversion (%) |
|---|---|---|---|---|
| Ru/C | 2.1 | 1.3 | 1.6 | 17 |
| | 7.0 | 3.1 | 2.3 | 60 |
| | 5.0 | 2.1 | 2.4 | 100 |
| Ru/$Al_2O_3$ | 2.1 | 2.0 | 1.1 | 27 |
| | 3.5 | 3.5 | 1.0 | 41 |
| | 4.5 | 4.4 | 1.0 | 67 |
| | 3.0 | 7.5 | 0.4 | 100 |

**Fig. 4** Comparison of PPE and product concentration (by family) in the hydroprocessing of PPE using Ru/C and Ru/Al$_2$O$_3$ catalysts at W·t = 100 mg h (Reaction conditions: 25 bar-g of H$_2$, 150 °C)

aromatic monomers produced through the corresponding route, and as conversion increased and these monomers started to suffer saturation, each term also included the corresponding saturated monomers (monomers produced through $k_4$ and $k_5$, or $k_6$-$k_{10}$).

$$R = \frac{moles \ of \ products \ from \ k_1}{moles \ of \ products \ from \ k_2} \qquad (6)$$

$R$ was calculated for each catalyst at comparable levels of conversion (Table 2), and it was observed that, for each of the three conversion levels considered (ca. 20%, ca. 60%, and 100%), the ratio obtained was higher with Ru/C than with Ru/Al$_2$O$_3$. These results confirm the fact that $k_1$ and $k_2$ routes are nearly equivalent in the Ru/C catalyst, whereas, $k_1$ is less favored in Ru/Al$_2$O$_3$. Recently, Wang and Liu [49] reported

DFT-calculated values of bond dissociation energies for the homolytic cleavage of $o$-OCH$_3$ substituted phenethyl phenyl ether. Although the actual values of such energies for the non-substituted dimer would differ from the calculated values, they can be taken as a reference to show that the cleavage of the C$_{aryl}$-O bond ($k_1$) requires more energy than the rupture of the C$_\beta$-O bond ($k_2$). Thus, it might be said that Ru/C enhances $k_1$. One could tentatively assign the higher selectivity to the C$_{aryl}$-O hydrogenolysis to electronic effects. Moreover, it could be proposed that on the under-coordinated Ru atoms located at surface defects, it will be possible to reduce the energetic barriers of the C$_{aryl}$-O hydrogenolysis, resulting in a higher selectivity to benzene and benzylethanol.

On the other hand, it can be observed that the $R$ value for Ru/C was ca. 1, except when conversion of the model compound was close to 100%. This was a consequence of the lower concentration of 2-phenylethan-1-ol and the higher concentration of ethylbenzene obtained, when compared to expected values. In general, monomers from $k_1$ route were obtained in a nearly 1:1 proportion (benzene and/or cyclohexanol: 2-phenylethanol and/or cyclohexaneethanol). The same applied for $k_2$ products. The lower concentration of 2-phenylethan-1-ol compared to the expected one can be attributed to the conversion of this compound into ethylbenzene. Dehydration of 1-phenylethanol to styrene has been reported in several reductive media [50, 51], and even though the dehydration of 2-phenylethan-1-ol seems to occur slower, it has also been reported to be converted into styrene [52]. Then, styrene could have undergone further hydrogenation to ethylbenzene [53].

Interestingly, when comparing $k_3$ and $k_3'$ routes, the latter seemed to be dominant when compared to the former for both

**Fig. 5** Proposed reaction network for hydroprocessing of PPE in methanol. Catalyst: 5% Ru/C or 5% Ru/Al$_2$O$_3$; 25 bar-g of H$_2$, 150 °C
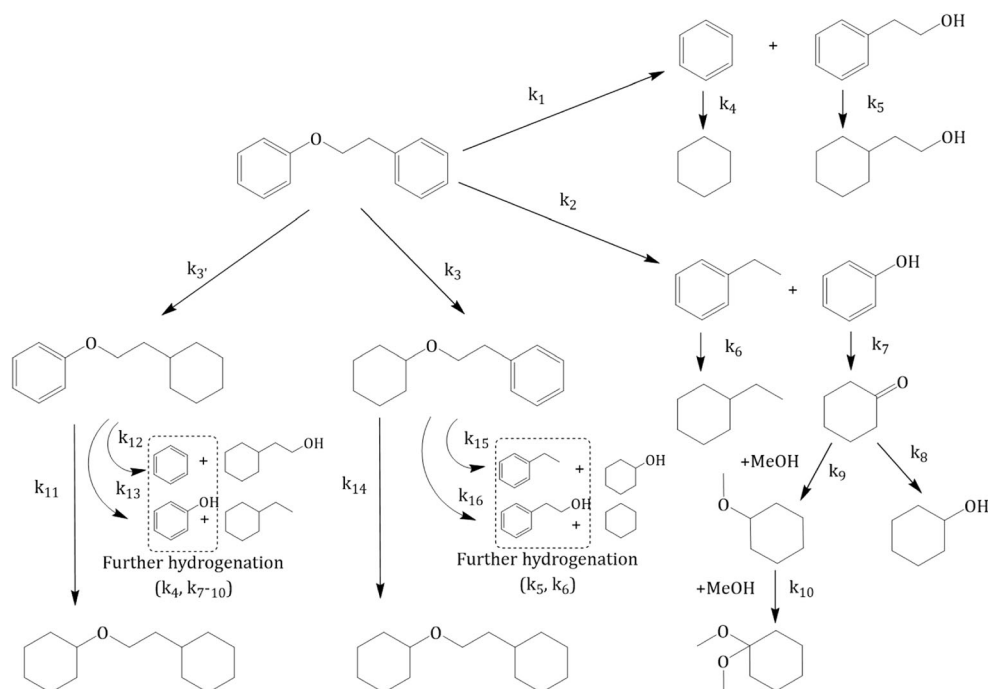
**Table 2** Calculation of the *R* parameter at different conversion levels for PPE hydroprocessing reactions using Ru/C and Ru/Al$_2$O$_3$ as catalysts. Reaction conditions: 25 bar-g of H$_2$, 150 °C

| Catalyst | Parameters | | | |
|---|---|---|---|---|
| 3.8% Ru/C | Conversion (%) | 19 | 61 | 100 |
| | *R* | 1.13 | 1.14 | 0.61 |
| 3.9% Ru/Al$_2$O$_3$ | Conversion (%) | 23 | 65 | 100 |
| | *R* | 0.14 | 0.05 | 0.15 |

catalysts. The calculated concentration of partially saturated dimer (2-cyclohexylethoxy)benzene was nearly 2.7 times greater than that of (2-(cyclohexylolxy)ethyl)benzene using Ru/C as catalyst, and 3–4 times greater with Ru/Al$_2$O$_3$, depending on the conversion level (conversion <100% in all commented cases). In the cases of ca. 100% of conversion, the differences between these two compounds were even more accentuated: with Ru/Al$_2$O$_3$, the concentration of (2-cyclohexylethoxy)benzene was over nine times that of (2-(cyclohexylolxy)ethyl)benzene; whereas with Ru/C the latter compound was not even detected at 100% of conversion, which might be due to its conversion to the fully saturated dimer.

Finally, it seems that fully hydrogenated dimers did not undergo further C-O cleavage reactions. Song et al. [54] studied the hydroprocessing of PPE using several C supported catalysts in methanol. With similar reaction conditions to those presented in this work (150 °C, 2 MPa of H$_2$, 2 h of reaction), they reported that over 3.8 wt. % Ru/C catalyst, fully hydrogenated PPE accounted for 60% of total products (>99% conversion). Consequently, under those conditions, it was concluded that hydrogenation of benzene rings was a dominant pathway compared to C-O bond cleavage. The same observation has been reported on heteronuclear aromatic molecules [55, 56]. The ring-opening reaction of furanic compounds involves hydrogenolysis of the C-O bond of the aromatic ring. The authors reported that the reaction rate of the

ring opening was significantly slower on saturated tetrahydrofuran compared to the furfural. They suggested that the interaction of the aromatic ring with the metal surface of the Ni catalyst was critical for the activation of the C-O bond.

**Study of the effect of reaction temperature** Finally, the effect of reaction temperature was briefly studied, also using Ru/Al$_2$O$_3$ and Ru/C as catalysts. Keeping H$_2$ pressure constant at 25 bar-g, reactions were carried out at 100 °C, 125 °C, and 150 °C. The results in terms of yield to the different families of compounds previously described are presented in Fig. 6.

Firstly, the results obtained using Ru/C will be discussed (Fig. 6, left). The three experiments were carried out at W·*t* = 100 mg·h, obtaining ca. 100% of PPE conversion in all cases. The results presented in Fig. 6, left seem to indicate that the change of reaction temperature within the studied values at the tested experimental conditions influenced product distribution, rather than the obtained level of conversion. For instance, hydrogenation of PPE rings (full or partial) seems to be more important at 100 °C than at 125 or 150 °C. In addition, the complete hydrogenation of all products, both dimers and monomers, at 125 °C is a significant result. Regarding Ru/Al$_2$O$_3$ results (Fig. 6, right), reactions at 100 and 150 °C were carried out at W·*t* = 100 mg·h, while the reaction at 125 °C was carried out at W·*t* = 134 mg·h. In all the experiments, conversion values were nearly 25–30%, being variations attributed to experimental deviations. In this case, it can also be concluded that temperature changes affected product distribution, being conversions around the same values. As shown in Fig. 6, right, the yield to monomers (aromatics in this case) increased with temperature, while the yield to fully and partially saturated dimers was reduced. In a recent study, Luo et al. [57] reported the hydrodeoxygenation of PPE using several Ru-based catalysts in water. They observed that at low temperatures (120–200 °C), hydrogenolysis of the C-O bond and hydrogenation of PPE were competing pathways.



**Fig. 6** Study of the effect of reaction temperature in PPE hydroprocessing. Catalysts: Left) Ru/C, Right) Ru/Al$_2$O$_3$
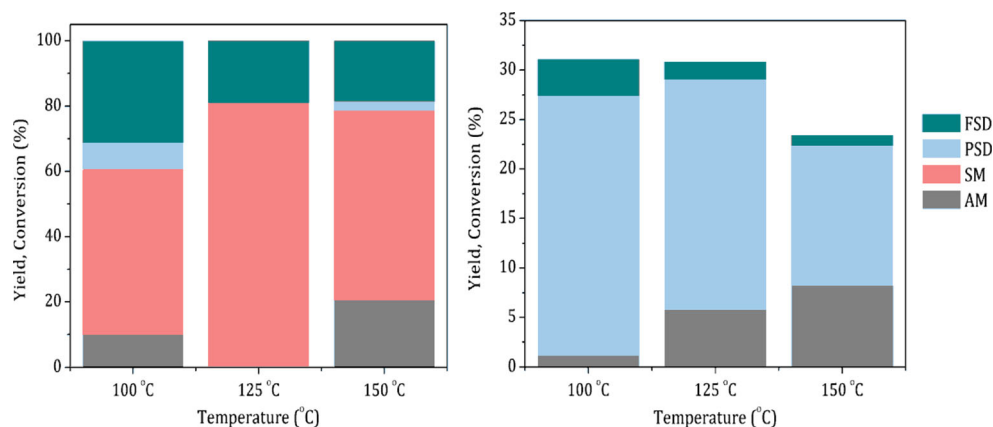
At temperatures under 140 °C, hydrogenation was even more important than hydrogenolysis, and it was not until 200 °C or above that hydrogenolysis was clearly the major route (>95% yield). Also, the same study reported that high hydrogen pressures (> 10 bar) also favored hydrogenation versus hydrogenolysis. High temperature and low hydrogen pressure were then concluded to have a beneficial effect for hydrogenolysis of PPE. This behavior was attributed to a preferential adsorption of $H_2$ on the metal catalyst around the oxygen atom of PPE, being the rest of $H_2$ preferentially desorbed from the catalyst at high temperatures [57, 58], and thus working against ring hydrogenation. Although the reaction media was different to the one used in this study, this tendency resembles that of $Ru/Al_2O_3$ (Fig. 6, right). Clearly, increasing temperatures in the 100–150 °C range promoted hydrogenolysis of PPE, as higher yields to aromatic monomers were obtained; whereas, the yield to fully and partially saturated dimers was decreased. On the other hand, at 150 °C, full or partial hydrogenation of PPE was still highly significant for the $Ru/Al_2O_3$ catalyst. Following again the results reported by Luo et al. [57], it seems that 150 °C was still a low temperature to enhance hydrogenolysis to be the major route, but more importantly, the high hydrogen pressure (25 bar-g) was more likely the main cause for strong PPE hydrogenation. Concerning the results obtained with Ru/C, this catalyst presents a higher intrinsic activity towards hydrogenolysis of the PPE C-O bonds when compared to $Ru/Al_2O_3$. Nevertheless, some of the aforesaid effects of temperature and pressure can also be observed in these experiments. The share of hydrogenolysis and hydrogenation was similar at 125 and 150 °C, but the former increased its importance at 100 °C. In addition, it can also be proposed that, when compared to the results observed at 150 °C with similar levels of hydrogenation of PPE and its hydrogenolysis, the higher hydrogenation of monomers at 125 °C could have been related to a higher $H_2$ coverage of the catalyst at low temperature. Per the observed results, temperature and $H_2$ pressure effect on product selectivity will need to be further investigated.

**Kinetic study** To further investigate the preferential routes observed for each catalyst, a preliminary kinetic model for both cases has been proposed to represent the results presented previously. The reaction network was complex, with several reactions taking place in series and in parallel, and also the same compound being formed and consumed in several steps. Therefore, as a first approach, constants $k_1$, $k_2$, $k_3$, and $k_3'$ were calculated according to the model proposed in Eqs. 7 and 8. Such calculations were performed by using data corresponding to the lowest levels of conversion, where saturated monomers or fully saturated dimer concentration were either non-detected or very low, to obtain the values of such constants for the first steps of the reaction. In addition, it was assumed that all reactions were of first order kinetics with respect to PPE (Eqs. 7 and 8).

$$\frac{\Delta C_{PPE}}{\Delta(W \cdot t)} = -r_1 - r_2 - r_3 - r_3' \tag{7}$$

$$r_1 = k_1 \cdot C_{PPE_{Wti}}; r_2 = k_2 \cdot C_{PPE_{Wti}}; r_3 = k_3 \cdot C_{PPE_{Wti}}; r_3'$$
$$= k_3' \cdot C_{PPE_{Wti}} \tag{8}$$

For Ru/C, calculations were carried out up to $W \cdot t = 50$ mg·h (60% of conversion); and for $Ru/Al_2O_3$ with data until $W \cdot t = 100$ mg·h (23% of conversion). The obtained values for the four constants in each case are presented in Table 3.

In the case of Ru/C, for the second experimental data point ($W \cdot t = 60$ mg h) 1.1-dimethoxycyclohexane was already detected. Thus, to calculate the four kinetic constants presented in Table 2, an additional constant was included to consider the initial amount of such compound. Routes including $k_7$ to $k_9$ in Fig. 5 were grouped under $k_7'$, assuming that the conversion of phenol to cyclohexanone, to 1-methoxycyclohexane, and to 1.1-dimethoxycyclohexane was fast. Calculated $k_7'$ value was $1.82 \times 10^{-2}$ s$^{-1}$. On the other side, initial kinetic constants for $Ru/Al_2O_3$ were calculated using only the first conversion point. The reason for this was that, even at 40% of conversion, plenty of saturated compounds were observed, and thus, the simplification of only including $k_1$, $k_2$, $k_3$, and $k_3'$ in the model was no longer acceptable.

The calculated values (Table 3) agreed with the results presented previously. As commented before, $k_1$ and $k_2$ routes seemed almost equivalent for Ru/C; whereas for $Ru/Al_2O_3$, the $k_2$ route was the dominant pathway. In this sense, the calculated values for these constants were nearly similar for Ru/C, whereas in the case of $Ru/Al_2O_3$ $k_2$ was ca. 4.5 times greater than $k_1$. Moreover, such constants were nearly one order of magnitude greater for Ru/C.

With regard to $k_3$ and $k_3'$, it was foreseen that $k_3'$ values would be higher than $k_3$ ones as the concentration of 2-(cyclohexyloxy)ethyl)benzene was greater with both catalysts regardless of the conversion level. Calculations showed that $k_3'$ values were nearly double to those of $k_3$ for both Ru/C and $Ru/Al_2O_3$. $k_3'$ was specifically 1.98 and 2.37 times $k_3$, respectively. The calculated values for these constants ($k_1$, $k_2$, $k_3$, and $k_3'$) were then fixed as constants, calculating afterwards the value for the rest of $k$'s. The values obtained for such parameters are collected in Table 4, first column of each catalyst (f) refers to parameters calculated keeping $k_1$–$k_3'$ constants from previous calculations; whereas, the second column (v) presents the same parameters calculated without fixing those four $k$ values. In the case of Ru/C, cyclohexanone was not detected in any of the experiments. Thus, two new constants, $k_8'$ and $k_{10}'$, were defined to represent the conversion of phenol to cyclohexanol ($k_8'$) and phenol to 1.1-dimethoxycyclohexane

**Table 3** Calculated kinetic constants for the first steps of PPE catalytic hydroprocessing

| Catalyst | $k_1$ (s$^{-1}$) | $k_2$ (s$^{-1}$) | $k_3$ (s$^{-1}$) | $k_3'$ (s$^{-1}$) |
|---|---|---|---|---|
| Ru/C | $2.97 \cdot 10^{-3}$ | $2.70 \cdot 10^{-3}$ | $1.87 \cdot 10^{-3}$ | $3.71 \cdot 10^{-3}$ |
| Ru/Al$_2$O$_3$ | $1.56 \cdot 10^{-4}$ | $6.98 \cdot 10^{-4}$ | $4.59 \cdot 10^{-4}$ | $1.09 \cdot 10^{-3}$ |

($k_{10}'$). For experiments with Ru/Al$_2$O$_3$, cyclohexanone was detected, and thus, $k_7$ and $k_8$ represent the aforesaid routes, while $k_{10}''$ was defined to represent the conversion of cyclohexanone into 1.1-dimethoxycyclohexane (1-methoxycyclohexane was not detected). Steps represented by $k$'s above $k_3'$ ($k_4$ to $k_{16}$) were also considered to be first order with respect to their corresponding reactant (for example, $k_4$ was calculated considering the hydrogenation of benzene to cyclohexane to be first-order kinetics with respect to benzene).

Before delving into the kinetic results, it should be noticed that the residual sum of squares (RSS) of any of the presented data fitting was considerably higher than desired. Specifically, RSS presented values of 36.18 and 13.16 for Ru/C (f) and Ru/Al$_2$O$_3$ (f), respectively, which decreased to 27.30 and 8.11 when variation of $k_1$, $k_2$, $k_3$, and $k_3'$ was considered. As shown in Fig. 7, the correlation coefficient ($r^2$) of the kinetic models for PPE hydrotreating on Ru/C varied from 0.908 to 0.930, and 0.974 to 0.985 for Ru/Al$_2$O$_3$, for the "fixed" and "variable" K-models, respectively. The elevated values of RSS and low $r^2$ evidence that the proposed model is not accurate enough to represent the complex reaction network and

reaction mechanism, as it will be discussed afterwards. Thus, these results should be taken with care and only as a preliminary approach to the kinetics of the studied system. Experimental concentration for each reaction product and the corresponding model-predicted values are presented in Figs. 8 and 9. Data reported in such figures correspond to models with allowed $k_1$–$k_3'$ variation, as differences between the values of such constants were small compared to the fixed values, and in turn, this led to a better overall fit of the model.

From the data reported in Table 4, it can be observed that $k_4$ and $k_5$ (corresponding to benzene and 2-phenylethan-1-ol saturation) values were nearly one, or even two, orders of magnitude greater in all cases, compared to $k_1$–$k_3'$ in the same model. This confirms the observed behavior of aromatic monomer hydrogenation, as once the aromatic monomers were formed through PPE's C-O bond cleavage; they were quickly saturated. Moreover, $k_8'$ and $k_{10}'$, constants for the conversion over Ru/C of phenol into cyclohexanol and 1.1-dimethoxycyclohexane, respectively, presented values one order of magnitude higher than constants for C-O cleavage or PPE saturation as well. Regarding Ru/Al$_2$O$_3$, similar values were observed for $k_7$ and $k_8$. In contrast, 1.1-dimethoxycyclohexane formation ($k_{10}''$) when using Ru/Al$_2$O$_3$ as catalyst was much slower, and nearly the range of $k_1$–$k_3'$ values. The latter connects with the lower concentrations of 1.1-dimethoxycyclohexane observed throughout the experiments carried out with Ru/Al$_2$O$_3$ when compared to Ru/C.

Furthermore, it can be observed that $k_6$ values were lower than those of the other constants representing the

**Table 4** Calculated kinetic constants for the proposed model (hydroprocessing of PPE, 150 °C)

| Constant (s$^{-1}$) | Ru/C (f) | Ru/C (v) | Ru/Al$_2$O$_3$ (f) | Ru/Al$_2$O$_3$ (v) |
|---|---|---|---|---|
| $k_1$ | $2.97 \times 10^{-3}$ | $2.94 \times 10^{-3}$ | $1.56 \times 10^{-4}$ | $1.76 \times 10^{-4}$ |
| $k_2$ | $2.70 \times 10^{-3}$ | $2.82 \times 10^{-3}$ | $6.98 \times 10^{-4}$ | $5.95 \times 10^{-4}$ |
| $k_3$ | $1.87 \times 10^{-3}$ | $3.29 \times 10^{-3}$ | $4.59 \times 10^{-4}$ | $4.41 \times 10^{-4}$ |
| $k_3'$ | $3.71 \times 10^{-3}$ | $5.22 \times 10^{-3}$ | $1.09 \times 10^{-3}$ | $8.68 \times 10^{-4}$ |
| $k_4$ | $2.91 \times 10^{-2}$ | $2.44 \times 10^{-2}$ | $1.25 \times 10^{-2}$ | $1.22 \times 10^{-2}$ |
| $k_5$ | $3.37 \times 10^{-2}$ | $3.38 \times 10^{-2}$ | $2.21 \times 10^{-3}$ | $2.79 \times 10^{-3}$ |
| $k_6$ | $1.68 \times 10^{-3}$ | $1.42 \times 10^{-3}$ | $1.36 \times 10^{-3}$ | $9.73 \times 10^{-4}$ |
| $k_7$ | – | – | $3.12 \times 10^{-3}$ | $4.05 \times 10^{-3}$ |
| $k_8$ | – | – | $5.42 \times 10^{-3}$ | $3.17 \times 10^{-3}$ |
| $k_8'$ | $2.35 \times 10^{-2}$ | $2.05 \times 10^{-2}$ | – | – |
| $k_{10}'$ | $1.99 \times 10^{-2}$ | $2.01 \times 10^{-2}$ | – | – |
| $k_{10}''$ | – | – | $1.69 \times 10^{-4}$ | $1.18 \times 10^{-4}$ |
| $k_{11}$ | $1.09 \times 10^{-2}$ | $1.11 \times 10^{-2}$ | $4.41 \times 10^{-4}$ | $3.85 \times 10^{-4}$ |
| $k_{12}$ | 0 | $9.23 \times 10^{-6}$ | $1.56 \times 10^{-4}$ | $7.98 \times 10^{-5}$ |
| $k_{13}$ | $1.98 \times 10^{-2}$ | $1.70 \times 10^{-2}$ | 0 | 0 |
| $k_{14}$ | $5.79 \times 10^{-3}$ | $4.66 \times 10^{-3}$ | $1.01 \times 10^{-4}$ | $3.14 \times 10^{-4}$ |
| $k_{15}$ | $9.53 \times 10^{-3}$ | $9.49 \times 10^{-3}$ | $2.18 \times 10^{-3}$ | $2.18 \times 10^{-3}$ |
| $k_{16}$ | $2.49 \times 10^{-2}$ | $2.30 \times 10^{-2}$ | $2.01 \times 10^{-4}$ | $2.01 \times 10^{-4}$ |

$f$ fixed constants, $v$ variable constants

**Fig. 7** Comparison of experimental and calculated concentration values obtained using the kinetic model with "variable" (*i*)) and "fixed" (*ii*)) for Ru/C (**a**) and Ru/Al$_2$O$_3$ (**b**)
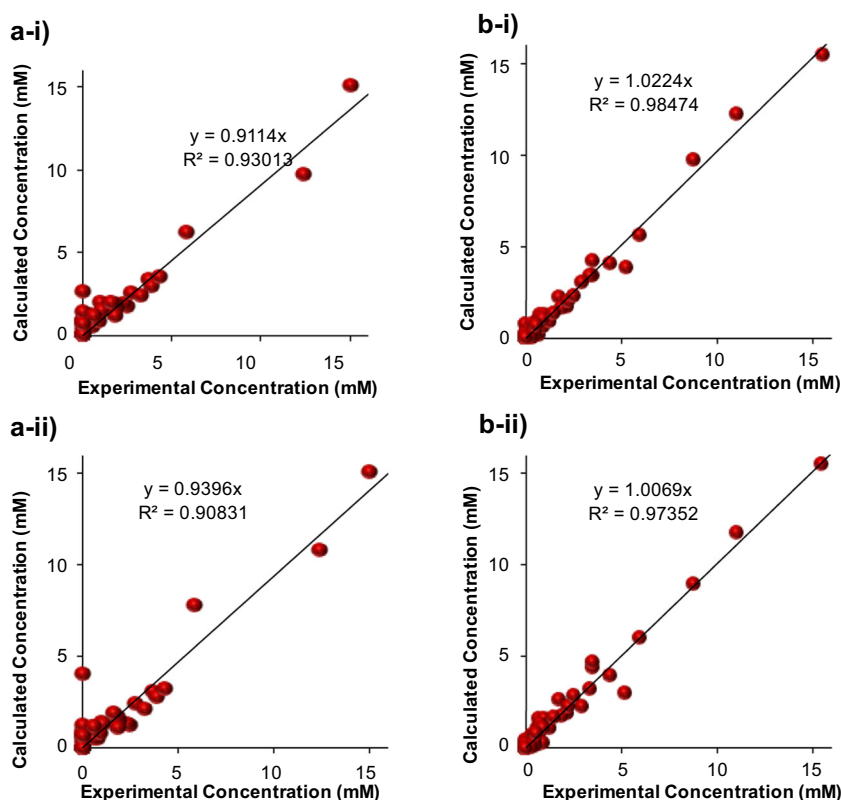


hydrogenation of aromatic monomers ($k_4$, $k_5$, $k_8'$, and $k_{10}'$ in the case of Ru/C; $k_4$, $k_5$, $k_7$, $k_8$ and $k_{10}''$ in the case of Ru/Al$_2$O$_3$). These values intended to model the experimental results in which it was observed that, while saturation of phenol (to cyclohexanol and/or 1.1-dimethoxycyclohexane due to the acetal reaction) was fast, the complementary monomer from the C-O scission (ethylbenzene) remained longer in the reaction media without being saturated (Figs. 8 and 9). Luo et al. [57] observed that phenol hydrogenation rate was much higher (96 mmol g$^{-1}$ h$^{-1}$) than that of ethylbenzene (7 mmol g$^{-1}$ h$^{-1}$) when they were co-introduced in aqueous reaction media to react over Ru/C catalysts. This behavior was attributed to a better solubility of phenol in water together with its preferential adsorption on the Ru particles, and such explanation could also be extended to the studied conditions in this work. Moreover, it should also be considered that the discussed pathway through which ethylbenzene could be formed from phenylethanol was not included in the presented kinetic models, and it can also contribute to higher ethylbenzene concentrations.

**Fig. 8** Experimental results (*scatter*-"exp") and kinetic model (*line*-"calc") using variable kinetic constants (v) for the hydroprocessing of PPE at 150 °C in methanol, 25 bar H$_2$, 750 rpm and 5% Ru/C as catalyst
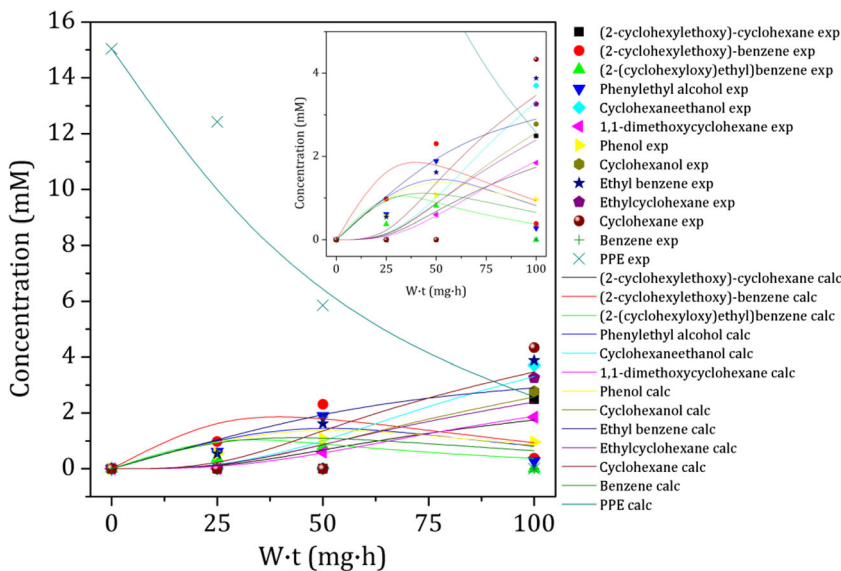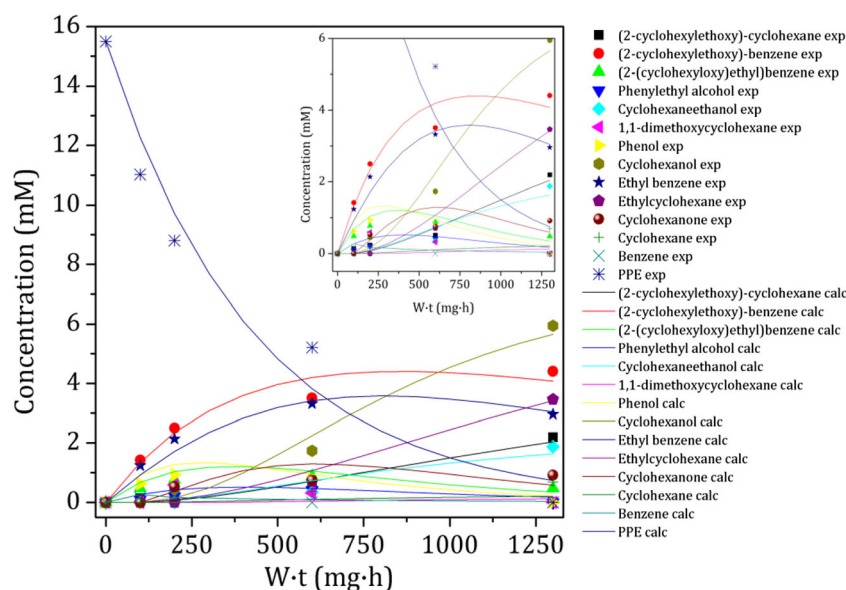
**Fig. 9** Experimental results (*scatter*-"exp") and kinetic model (*line*-"calc") using variable kinetic constants (v) for the hydroprocessing of PPE at 150 °C in methanol, 25 bar $H_2$, 750 rpm and 3.9% Ru/$Al_2O_3$ as catalyst



On the other hand, calculated kinetic constants for Ru/C are in general higher than the corresponding ones for Ru/$Al_2O_3$. It has already been commented that the former catalyst presented a higher activity for PPE conversion. When compared to Ru/$Al_2O_3$, the same value of conversion was achieved at lower $W{\cdot}t$ with Ru/C. For comparative purposes, the concentration of converted moles of the model compound per gram of catalyst and second were calculated at $W{\cdot}t$ = 100 mg h for both catalysts (Table 5). It was observed that this parameter was almost four times higher for Ru/C than for Ru/$Al_2O_3$. If we divide those values by the corresponding surface area of the catalyst (Table 5), the obtained values are of the same order of magnitude. This result clearly showed that the higher catalytic activity per mass of catalyst observed on Ru/C was due to the higher metal dispersion on the activated carbon surface. As part of a future study, it would be very interesting to test a Ru/$Al_2O_3$ catalyst with a higher surface area for comparison. Perhaps, that catalyst with high surface area and small Ru nanoparticles, and supported on alumina, may lead to better activity results.

In view of the results presented in Figs. 8 and 9, it can be concluded that, as already commented with calculated RSS values, the proposed model fitted better the experimental data obtained using Ru/$Al_2O_3$ as catalyst. General tendencies of consumption and formation of the different products and reactants were acceptably well described by the model, though some over/under estimation of concentrations was observed, for example with phenol. As for Ru/C, general trends were also predicted by the model, but the over/under estimation of concentrations was more accentuated. For instance, ethylbenzene was overestimated (Fig. 8) up to $W{\cdot}t$ = 50 mg h, and underestimated at higher $W{\cdot}t$. In addition, modeling of the evolution of partially saturated dimers or cyclohexane was also inaccurate. The case of ethylbenzene can be attributed to the production route of such compound from phenylethanol that, as commented before, was not included in the model. But, even though it is evident that the reaction mechanism with Ru/C as catalyst differs from that of Ru/$Al_2O_3$, Ru/C seemed to present intrinsic characteristics that modified the obtained product distribution.

A more accurate model will require a thorough modification of the proposed equations, including new terms that consider phenomena such as preferential adsorption of certain molecules on the catalyst surface, or varying the kinetic order of the elemental steps of the reaction. Such detailed study is beyond the scope of this work, as the purpose was to perform a preliminary approach to the kinetics of the studied system.

# 5 Conclusions

The reaction network for the hydrogenolysis of PPE with Ru/C and Ru/$Al_2O_3$ was studied. It was concluded that the first steps of the reaction included the hydrogenolysis of the $C_{\beta}$-O ether or the $C_{aryl}$-O bond and the saturation of one of the rings of PPE. After this, aromatic monomers produced from the rupture of the ether bond underwent further hydrogenation, and the partially saturated dimers either were cleaved to form the corresponding monomers or were fully saturated. Differences in

**Table 5** Converted moles of PPE per gram of catalyst and per second (left column), and the same value normalized by the surface area of the catalysts (right column)

| Catalyst | PPE converted (mol PPE/($g_{cat}{\cdot}$s)) | PPE converted (mol PPE/($m^2$s)) |
| --- | --- | --- |
| Ru/C | 0.83 | $1.02{\cdot}10^{-3}$ |
| Ru/$Al_2O_3$ | 0.22 | $0.95{\cdot}10^{-3}$ |

the relative importance of each of the commented pathways were observed from one catalyst to the other. The selectivity of hydrogenolysis changed as function of conversion. While the ratio of hydrogenolysis to hydrogenation products progressively increased as the reaction evolved using the Ru/C catalyst, the opposite was observed on the Ru/Al$_2$O$_3$. Notably, the selectivity between the hydrogenolysis of the C$_{aryl}$-O and C$_\beta$-O also varied with the catalyst. When Ru/Al$_2$O$_3$ was used as catalyst, the cleavage of the weaker C$_\beta$-O bond was a major pathway when compared to the cleavage of the C$_{aryl}$-O. Conversely, with Ru/C as catalyst, the cleavage of these two bonds was almost equivalent. These observations could be related to the higher reactivity of the low-coordination atoms present in a greater extent on the smaller Ru particles of the Ru/C compared to Ru/Al$_2$O$_3$.

With the proposed reaction network, a first approach to the kinetic modeling of the reaction was carried out. The proposed model fitted better the experimental data obtained using Ru/Al$_2$O$_3$ than that obtained with Ru/C as catalyst. General tendencies of consumption and formation of the different products and reactants were described by the model, though some over/under estimation of concentrations was observed, especially in the case of Ru/C. A more accurate model will require the modification of the equations used, considering additional terms accounting for phenomena such as adsorption competence between molecules.

Moreover, the effect of reaction temperature was studied, also using Ru/Al$_2$O$_3$ and Ru/C as catalysts. It was observed that decreasing temperature from 150 to 125 or 100 °C (at comparable levels of conversion) favored the dimer hydrogenation route versus the hydrogenolysis of the ether bonds. It was concluded that both temperature and H$_2$ pressure affected product selectivity and therefore, alternatives that allow increasing temperature while reducing H$_2$ pressure will be needed.

# References

1. Directorate general for research and innovation, Innovating for sustainable growth: A bioeconomy for Europe, European Comission, 2012, vol 8
2. Huber GW, Iborra S, Corma A (2006) Synthesis of transportation fuels from biomass: chemistry, catalysts, and engineering. Chem Rev 106:4044–4098
3. Serrano-Ruiz JC, Luque R, Clark JH (2013) The role of heterogeneous catalysis in the biorefinery of the future. In: Triantafyllidis K, Lappas A and Stöcker M (eds) The role of catalysis for the sustainable production of bio-fuels and bio-chemicals. Elsevier, pp 557–576
4. Serrano-Ruiz JC, Dumesic JA (2011) Catalytic routes for the conversion of biomass into liquid hydrocarbon transportation fuels. Energy Environ Sci 4:83–89
5. Rinaldi R, Schüth F (2009) Design of solid catalysts for the conversion of biomass. Energy Environ Sci 2:610–626
6. Gallezot P (2012) Conversion of biomass to selected chemical products. Chem Soc Rev 41:1538–1558
7. Menon V, Rao M (2012) Trends in bioconversion of lignocellulose: biofuels, platform chemicals & biorefinery concept. Prog Energy Combust Sci 38:522–550
8. Matson TC, Barta K, Iretskii AV, Ford PC (2011) One-pot catalytic conversion of cellulose and of woody biomass solids to liquid fuels. J Am Chem Soc 133:14090–14097
9. Anderson EM, Katahira R, Reed M, Resch MG, Karp EM, Beckham GT, Roman-Leshkov Y (2016) Reductive catalytic fractionation of corn stover lignin. ACS Sustain Chem Eng 4:6940–6950
10. Zhou CH, Xia X, Lin CX, Tong DS, Beltramini J (2011) Catalytic conversion of lignocellulosic biomass to fine chemicals and fuels. Chem Soc Rev 40:5588–5617
11. Resasco DE, Sitthisa S, Faria J, Prasomsri T, Ruiz MP (2011) Furfurals as chemical platform for biofuels production. In: Kubicka D, Kubicková I (eds) Heterogeneous catalysis in biomass to chemicals and fuels. Research Signpost, Kerala
12. Faria J, Ruiz MP, Resasco DE (2015) Carbon nanotube/zeolite hybrid catalysts for glucose conversion in water/oil emulsions. ACS Catal 5:4761–4771
13. Rico Campos A (2014) PhD Thesis, University of Seville (Spain)
14. Dias MOS, Junqueira TL, Cavalett O, Cunha MP, Jesus CDF, Mantelatto PE, Rossell CEV, Maciel R, Bonomi A (2013) Chemical engineering research and design cogeneration in integrated first and second generation ethanol from sugarcane. Chem Eng Res Des 91:1411–1417
15. Saidur R, Abdelaziz EA, Demirbas A, Hossain MS, Mekhilef S (2011) A review on biomass as a fuel for boilers. Renew Sustain Energy Res 15:2262–2289
16. Demirbas A (2005) Potential applications of renewable energy sources, biomass combustion problems in boiler power systems and combustion related environmental issues. Prog Energy Combust Sci 31:171–192
17. Deng W, Zhang H, Wu X, Li R, Zhang Q, Wang Y (2015) Oxidative conversion of lignin and lignin model compounds catalyzed by CeO2-supported Pd nanoparticles. Green Chem 17:5009–5018
18. Toledano A, Serrano L, Labidi J (2014) Improving base catalyzed lignin depolymerization by avoiding lignin repolymerization. Fuel 116:617–624
19. Erdocia X, Prado R, Corcuera MA, Labidi J (2014) Influence of reaction conditions on lignin hydrothermal treatment. Front Energy Res 2:1–7
20. Li C, Zhao X, Wang A, Huber GW, Zhang T (2015) Catalytic transformation of lignin for the production of chemicals and fuels. Chem Rev 115:11559–11624
21. Zakzeski J, Bruijnincx PCA, Jongerius AL, Weckhuysen BM (2010) The catalytic valorization of lignin for the production of renewable chemicals. Chem Rev 110:3552–3599
22. Azadi P, Inderwildi OR, Farnood R, King DA (2013) Liquid fuels, hydrogen and chemicals from lignin: a critical review. Renew Sust Energ Rev 21:506–523
23. Kärkäs MD, Matsuura BS, Monos TM, Magallanes G, Stephenson CRJ (2016) Transition-metal catalyzed valorization of lignin: the key to a sustainable carbon-neutral future. Org Biomol Chem 14:1853–1914

24. Xu C, Arancon RAD, Labidi J, Luque R (2014) Lignin depolymerisation strategies: towards valuable chemicals and fuels. Chem Soc Rev 43:7485–7500

25. He J, Zhao C, Lercher JA (2012) Ni-catalyzed cleavage of aryl ethers in the aqueous phase. J Am Chem Soc 134:20768–20775

26. Zhang C, Lu J, Zhang X, MacArthur K, Heggen M, Li H, Wang F (2016) Cleavage of the lignin β-O-4 ether bond via a dehydroxyl-ation–hydrogenation strategy over a NiMo sulfide catalyst. Green Chem. doi:10.1039/C6GC01456A

27. Dabral S, Mottweiler J, Rinesch T, Bolm C (2015) Base-catalysed cleavage of lignin β-O-4 model compounds in dimethyl carbonate. Green Chem 17:4908–4912

28. Strassberger Z, Alberts AH, Louwerse MJ, Tanase S, Rothenberg G (2013) Catalytic cleavage of lignin β-O-4 link mimics using copper on alumina and magnesia-alumina. Green Chem 15:768–774

29. Wang M, Li LH, Lu JM, Li HJ, Zhang XC, Liu HF, Luo NC, Wang F (2017) Acid promoted C–C bond oxidative cleavage of β-O-4 and β-1 lignin models to esters over a copper catalyst. Green Chem doi. doi:10.1039/C6GC02970A

30. Zhu G, Ouyang X, Yang Y, Ruan T, Qiu X (2016) Selective cleav-age of aryl ether bonds in dimeric lignin model compounds. RSC Adv 6:17880–17887

31. Davis RJ, Davis SE, Ide MS, Davis RJ (2013) Selective oxidation of alcohols and aldehydes over supported metal nanoparticles. Green Chem 15:17–45

32. Rodrigues EG, Pereira MFR, Chen X, Delgado JJ, Órfão JJM (2011) Influence of activated carbon surface chemistry on the ac-tivity of au/AC catalysts in glycerol oxidation. J Catal 281:119–127

33. Prasomsri T, Shi D, Resasco DE (2010) Anchoring Pd nanoclusters onto pristine and functionalized single-wall carbon nanotubes : a combined DFT and experimental study. Chem Phys Lett 497:103–107

34. Namdeo A, Mahajani SM, Suresh AK (2016) Palladium catalysed oxidation of glycerol - effect of catalyst support. J Mol Catal A Chem 421:45–56

35. Sarapatka J (1993) Pd-induced charge transports with Pd/Al₂O₃/al interface formation. J Phys Chem 97:11274–11277

36. Hicks RF, Fleisch TH, Bell AT (1984) An XPS study of metal-support interactions on Pd/SiO₂ and Pd/La₂O₃. J Catal 87:398–413

37. Rensel DJ, Rouvimov S, Gin ME, Hicks JC (2013) Highly selective bimetallic FeMoP catalyst for C-O bond cleavage of aryl ethers. J Catal 305:256–263

38. Mazzieri V, Coloma-Pascual F, Arcoya A, L'Argentière PC, Fígoli NS (2003) XPS, FTIR and TPR characterization of Ru/Al₂O₃ cat-alysts. Appl Surf Sci 210:222–230

39. Gaur S, Pakhare D, Wu H, Haynes DJ, Spivey JJ (2012) CO₂ reforming of CH₄ over Ru-substituted pyrochlore catalysts: effects of temperature and reactant feed ratio. Energy Fuel 26:1989–1998

40. Liang C, Wei Z, Luo M, Ying P, Xin Q, Li C (2001) Hydrogen spillover effect in the reduction of barium nitrate of Ru- Ba(NO₃)₂/ AC catalysts for ammonia synthesis. In: Guerrero-Ruiz A, Rodriguez-Ramons I (eds) Studies in Surface Science and Catalysis, vol 138. Elsevier Masson SAS, Paris, pp 283–290

41. Zhu L, Yin S, Yin Q, Wang H, Wang S (2015) Biochar: a new promising catalyst support using methanation as a probe reaction. Energy Sci Eng 3:126–134

42. Xiong J, Dong X, Li L (2012) CO selective methanation in hydrogen-rich gas mixtures over carbon nanotube supported Ru-based catalysts. J Nat Gas Chem 21:445–451

43. He J, Zhao C, Lercher JA (2014) Impact of solvent for individual steps of phenol hydrodeoxygenation with Pd/C and HZSM-5 as catalysts. J Catal 309:362–375

44. Thomas B, Prathapan S, Sugunan S (2005) Synthesis of dimethyl acetal of ketones: design of solid acid catalysts for one-pot acetalization reaction. Microporous Mesoporous Mater 80:65–72

45. Lopez-Ramon MV, Stoeckli F, Moreno-Castilla C, Carrasco-Marin F (1999) On the characterization of acidic and basic surface sites on carbons by various techniques. Carbon 37:1215–1221

46. Regalbuto JR, Schrier M, Hao X, Spieker WA, Kim JG, Miller JT et al (2002) Toward a molecular understanding of noble metal cat-alyst impregnation. Elsevier Masson SAS, Paris

47. Arico AS, Antonucci V, Minutoli M, Giordano N (1989) The influ-ence of functional groups on the surface acid-base characteristics of carbon blacks. Carbon 27:337–347

48. Horst J, Holl WH (1997) Application of the surface complex for-mation model to ion exchange equilibria. J Colloid Interface Sci 195:250–260

49. Wang M, Liu C (2016) Theoretic studies on decomposition mech-anism of o-methoxy phenethyl phenyl ether: primary and secondary reactions. J Anal Appl Pyrol 117:325–333

50. Lange J, Otten V (2007) Dehydration of phenyl-ethanol to styrene under reactive distillation conditions: understanding the catalyst deactivation. Ind Eng Chem Res 46:6899–6903

51. Korstanje TJ, Jastrzebski JTBH, Klein RJM (2010) Catalytic dehy-dration of benzylic alcohols to styrenes by rhenium complexes. ChemSusChem 3:695–697

52. US Patent 2009/0187055 A1, 2009

53. L'Argentiere P, Figoli NS (1990) Regeneration of a sulfur poisoned Pd/Al₂O₃ catalyst during the selective hydrogenation of styrene. Appl Catal 61:275–282

54. Song Q, Cai J, Zhang J, Yu W, Wang F, Xu J (2013) Hydrogenation and cleavage of the C-O bonds in the lignin model compound phenethyl phenyl ether over a nickel-based catalyst. Chinese J Catal 34:651–658

55. Sitthisa S, Resasco DE (2011) Hydrodeoxygenation of furfural over supported metal catalysts: A comparative study of Cu , Pd and Ni. Catal Lett 141:784–791

56. Sitthisa S, Sooknoi T, Ma Y, Balbuena PB, Resasco DE (2011) Kinetics and mechanism of hydrogenation of furfural on cu/SiO₂ catalysts. J Catal 277:1–13

57. Luo Z, Wang Y, He M, Zhao C (2016) Precise oxygen scission of lignin derived aryl ethers to quantitatively produce aromatic hydro-carbons in water. Green Chem 18:433–441

58. Jerkiewicz G (2010) Electrochemical hydrogen adsorption and ab-sorption. Part 1: under-potential deposition of hydrogen. Electrocatalysis 1:179–199